# Chapter 5

# 2D Drift-Wave Model

The turbulent cascade of fluctuation energy to small scales is analogous in some ways to the transfer of fluctuation energy to fine velocity scales through phase-space mixing. The transfer of energy in turbulence can be very nonlinear in character in some situations (the inverse energy cascade in 2D, for example). There are limits, however, where the stretching of small-scale eddies by long wavelengths is similar in character to the passive phase mixing of the Vlasov equation. The basic physical scaling of damping to transfer of fluctuation energy to small scales that is discussed in Chapter 3 will be used in Chapter 6 to develop nonlinear viscosity models that model the transfer of fluctuation energy in drift turbulence due to flow shear.

The chief goal of developing subgrid turbulence models for drift-wave turbulence is to improve the accuracy of comprehensive 3D turbulence simulations. In order to effectively study the physics of fluctuation transfer in a simplified situation, however, the initial research of this thesis focuses on a 2D model problem. The model equation for this study was chosen to be as simple as possible while retaining the basic physics relevant to subgrid turbulence processes in fluid simulations of drift wave turbulence.

Saturation in toroidal gyrofluid turbulence simulations (Beer 1995) involves a balance between the source of fluctuations in linearly unstable modes and the dissipation in modes that are stabilized by terms that model Landau damping. Fluctuation energy is transferred from unstable to stable modes through the advection nonlinearity. A useful 2D model will at least contain the $\mathbf{E}\times\mathbf{B}$ drift advection nonlinearity, a linear instability, and dissipation to model Landau damping, which is primarily a function of the parallel wavelength and should therefore be present at long perpendicular wavelengths. The system presented here includes models of these three essential effects; however, it is a relatively simple one-field 2D equation resulting from major approximations. For example, it does not model bad curvature and ion temperature dynamics, which are important instability mechanisms in the core region of many tokamaks. As a 2D model, it is missing a special constraint on the adiabatic electron response, which enhances the role of the $k_y = k_z = 0$ component of the electrostatic potential (Dorland 1993), leading to turbulence-generated sheared flows that are important in toroidal simulations (Hammett et al. 1993; Beer 1995; Dimits et al. 1994; Waltz et al. 1994). Nevertheless, the system used in this study is a useful paradigm for studying certain effects important in plasma turbulence where the $\mathbf{E}\times\mathbf{B}$ nonlinearity is important, and some of the lessons learned in this simple model can then be applied in more complicated 3D multi-field simulations.

## 5.1 Model Equation

There is a significant literature on 2D models for drift-wave turbulence. The prototypical model of Hasegawa and Mima (1978) captures the basic physics of the $\mathbf{E}\times\mathbf{B}$ nonlinearity in a one-field 2D equation, but contains no linear drive to produce fluctuations. A model of linear drive is introduced in so-called "$i\delta$" equations (Terry and Horton 1982; Liang et al. 1993) through a simple model for the non-adiabatic part of the electron response. The model equation derived here is a simplified $i\delta$ model, with an additional term added to model Landau damping at long wavelengths.

There are a number of derivations in the literature of this model starting from standard fluid equations. Here the derivation is sketched from a gyrokinetic/gyrofluid perspective. The starting point is just a conservation equation for the ion-guiding-center density $n_{gc}$,

$$\frac{\partial n_{gc}}{\partial t} + \boldsymbol{\nabla} \cdot [n_{gc}(\mathbf{V}_{\mathbf{E}\times\mathbf{B}} + u_{\|}\hat{\mathbf{z}})] = 0, \tag{5.1}$$

where

$$\mathbf{V}_{\mathbf{E}\times\mathbf{B}} = \frac{c}{B}\hat{\mathbf{z}}\times\boldsymbol{\nabla}\phi \tag{5.2}$$

is the $\mathbf{E}\times\mathbf{B}$ drift velocity, $\phi$ is the potential, and $u_{\|}$ is the parallel ion flow. The ion FLR effects are ignored (via the assumption $T_i \ll T_e$) while the ion polarization effects are retained by including the ion polarization density in addition to the guiding-center density in determining the actual ion density

$$n_i = n_{gc} + n_0\frac{\rho_s^2 e}{T_e}{\boldsymbol{\nabla}_{\perp}}^2\phi, \tag{5.3}$$

where $\rho_s = c_s/\Omega_{ci}$ is the gyroradius using the ion gyrofrequency $\Omega_{ci} = eB/m_i c$, and the sound speed is $c_s = \sqrt{T_e/m_i}$. (This approach is the standard method used in the gyrokinetic Poisson equation (Lee 1983; Dubin et al. 1983; Lee 1987).) For the ion parallel flow velocity, the "1-moment" model of Landau damping,

$$n_0\frac{d}{dz}u_{\|} \approx C_1 v_t|k_{\|}|(n+\phi) \approx C_2 v_t|k_{\|}|n, \tag{5.4}$$

of Dorland and Hammett (1993) is used, where $C_1$ and $C_2$ are constants of order unity. Making use of the standard two-scale approximations to expand $n_{gc}$ in Eq. (5.1) via

$$n_{gc} = n_0\left(1 + \frac{x - x_0}{L_n}\right) + \tilde{n}_i \tag{5.5}$$

into a long-scale equilibrium part with density gradient scale length, $L_n$, and a short-scale fluctuating component $\tilde{n}_i$, leads to

$$\frac{\partial \tilde{n}_i}{\partial t} + \mathbf{V}_{\mathbf{E}\times\mathbf{B}} \cdot \boldsymbol{\nabla} \tilde{n}_i + n_0 V_d \frac{\partial}{\partial y}\left(\frac{e\phi}{T_e}\right) = -\alpha \frac{c_s}{L_n}\tilde{n}_i + \mu \frac{c_s {\rho_s}^2}{L_n} {\boldsymbol{\nabla}_\perp}^2 \tilde{n}_i, \tag{5.6}$$

where the diamagnetic drift velocity, $V_d = c_s\rho_s/L_n$, has been introduced. The density gradient in the long-scale equilibrium is responsible for the introduction of the diamagnetic drift term. The viscosity-like term containing $\mu$ is included to provide a sink for fluctuation energy at high $k$. The Landau damping model introduces the dissipative term $-\alpha c_s \tilde{n}_i/L_n$, where $\alpha$ is set to $C_2 v_t |k_\|| L_n/c_s$ for a typical small but finite $k_\|$ [$\sim (qR)^{-1}$ in a tokamak]. Three-dimensional simulations of drift-wave turbulence have found that the bulk of the dissipation comes from Landau damping (Beer 1995), so it is necessary to include a model for this process in 2D simulations where $k_\|$ has been ignored.

To close the model system, the fluctuation density must be related to the potential. The real-space ion density $\delta n_i$ is just the sum of the guiding space density $\tilde{n}_i$ and the ion polarization density ${\rho_s}^2 {\boldsymbol{\nabla}_\perp}^2 e\phi/T_e$. As a crude model for the electron response that will provide linear drive, we set $\delta n_e = (1 - \delta_0 \rho_s \partial/\partial y) e\phi/T_e$ (Terry and Horton 1982). Quasineutrality therefore gives us

$$\tilde{n}_i = \frac{n_0 e}{T_e}\left(1 - {\rho_s}^2 {\boldsymbol{\nabla}_\perp}^2 - \delta_0 \rho_s \frac{\partial}{\partial y}\right)\phi. \tag{5.7}$$

Upon using the normalized variables

$$\tau = \frac{c_s}{L_n} t, \quad x' = x\rho_s, \quad y' = y\rho_s, \quad \psi = \frac{L_n}{\rho_s}\frac{e}{T_e}\phi, \tag{5.8}$$

and then dropping the primes, we obtain the evolution equation

$$\left(\frac{\partial}{\partial \tau} + \alpha - \mu {\boldsymbol{\nabla}_\perp}^2\right)\left(1 - {\boldsymbol{\nabla}_\perp}^2 - \delta_0 \frac{\partial}{\partial y}\right)\psi + \hat{\mathbf{z}}\times\boldsymbol{\nabla}\psi \cdot \boldsymbol{\nabla}\left(-{\boldsymbol{\nabla}_\perp}^2 - \delta_0 \frac{\partial}{\partial y}\right)\psi + \frac{\partial \psi}{\partial y} = 0. \tag{5.9}$$

Expressing the potential as a sum of Fourier modes, $\psi = \sum_{\mathbf{k}} \exp(i\mathbf{k}\cdot\mathbf{x})\psi_{\mathbf{k}}$, gives the mode coupling equation

$$\left(\frac{\partial}{\partial \tau} + i\omega_{\mathbf{k}} - \gamma_{\mathbf{k}} - \gamma_{\mathbf{k}}^d\right)\psi_{\mathbf{k}} = N_{\mathbf{k}}, \tag{5.10}$$

where the nonlinear term is defined as

$$N_{\mathbf{k}} = \sum_{\mathbf{k}'} \frac{\hat{\mathbf{z}}\times\mathbf{k}' \cdot \mathbf{k}\left[|\mathbf{k}-\mathbf{k}'|^2 - i\delta_0(k_y - k'_y)\right]}{1 + |\mathbf{k}|^2 - i\delta_0 k_y}\,\psi_{\mathbf{k}'}\,\psi_{\mathbf{k}-\mathbf{k}'} \tag{5.11}$$

and the linear frequency and growth rate are given by

$$\omega_{\mathbf{k}} = \frac{k_y(1+|\mathbf{k}|^2)}{(1+|\mathbf{k}|^2)^2 + {\delta_0}^2 {k_y}^2}, \tag{5.12}$$

$$\gamma_{\mathbf{k}} = \frac{\delta_0 {k_y}^2}{(1+|\mathbf{k}|^2)^2 + {\delta_0}^2 {k_y}^2} - \alpha - \mu|\mathbf{k}|^2. \tag{5.13}$$

An additional growth rate $\gamma_{\mathbf{k}}^d$ has been introduced to contain one of the numerical dissipation models discussed in the following chapter. The true system that is being studied has $\gamma_{\mathbf{k}}^d = 0$, and with sufficiently high resolution the turbulent saturated state can be numerically simulated. Other dissipation models, to be defined later, can be used to improve the accuracy of simulations with insufficient resolution. [The dissipation models that will be considered are regular hyperviscosity (6.16), parameterized hyperviscosity (6.19), and the Smagorinsky eddy viscosity (6.5).] The linear physics of this model agrees with a model for dissipative trapped-electron drift waves derived by Liang et al. (1993) to first order in $\delta_0$ ($D_0$ in their notation) and second order in $k\rho_s$. Setting $\alpha = 0$, $\mu = 0$, and $\delta_0 = 0$ gives the equation of Hasegawa and Mima (1978).

The model equation used here was chosen for simplicity and only contains the gross features of drift-wave turbulence. To be of practical use, in fact, the results concerning eddy viscosity should not depend on the precise nature of Eq. (5.9), since we are interested in applications to more sophisticated models of drift-wave turbulence. The toroidal gyrofluid equations (Beer 1995; Waltz et al. 1992), which evolve multiple fields and contain significantly more complicated (hence more accurate) linear physics, share the same basic nonlinear advection term contained in this model. Hence the eddy viscosity calculated in this study is parameterized as a function of the advecting velocity without reference to the linear physics.

## 5.2 Physics of the Saturated State

Before considering the effects of the subgrid scales, we examine the results of simulating the model, Eq. (5.9), for a typical set of parameters. Simulations were performed with periodic boundary conditions using the standard dealiased pseudospectral approach. A hyperviscous damping term of the form discussed in the next section was used for the results considered here. Initially we consider a box of size $50\rho_s \times 50\rho_s$, using a $128\times128$ grid in real space, for parameters $\delta_0 = 0.35$, $\alpha = 0.035$, and $\mu = 0.0001$, with a hyperviscosity defined by Eq. (6.16) with power $p = 16$ and coefficient set to the average rate of shear, $\nu_h = S(t)$. [See Eq. (6.17).] This choice of $\delta_0$ gives growth rates large enough that the saturated state is in the strong-turbulence regime. [For this model equation, the wave frequencies are fixed, and the growth rates are proportional to the parameter $\delta_0$. For low growth rates, the total energy saturates at a level proportional to $\delta_0$. For large growth rates, the total energy in the saturated state

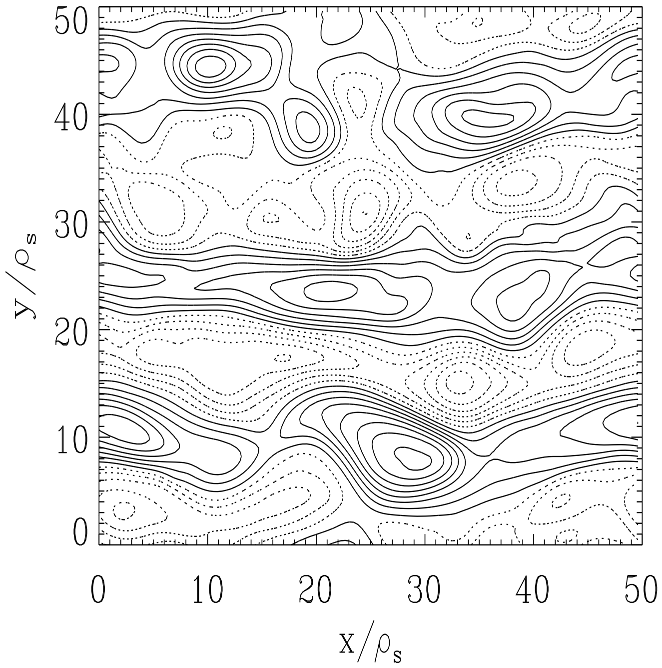


Figure 5.1: Contours of potential for saturated turbulence at one instant.

scales as ${\delta_0}^2$. For the purposes of this study, when the drive $\delta_0$ lies in the transition between these two scalings the simulations will be said to take place in the moderate-turbulence regime. The strong- and weak-turbulence regimes are defined respectively for larger and smaller values of the drive $\delta_0$. [Krommes and Hu (1994) discuss saturation levels for some simple drift-wave models.] The instantaneous potential late in the simulation is shown in Fig. 5.1.

One useful macroscopic parameter that can be expressed in this model is the volume-averaged particle flux

$$\begin{aligned}\Gamma &= \frac{1}{L_x L_y}\int_0^{L_x}\int_0^{L_y} \hat{\mathbf{x}}\cdot\mathbf{V}_{\mathbf{E}\times\mathbf{B}}\tilde{n}_i\,dy\,dx \\ &= \delta_0\left(\frac{\rho_s}{L_n}D_{\mathrm{B}}\right)\frac{n_0}{L_n}\sum_{\mathbf{k}}{k_y}^2|\psi_{\mathbf{k}}|^2.\end{aligned} \tag{5.14}$$

(The Bohm diffusivity, $D_{\mathrm{B}} = cT_e/eB$, has been introduced here.) The gyro-Bohm scaling of the flux is the natural scaling for this system, since the use of periodic boundary conditions and a constant background gradient prevents the system scale from directly entering the analysis. (The system scale could in principle enter through the size of the simulation domain $L_x \times L_y$, implying a Bohm scaling. The fact that "flux-tube" simulations saturate (Beer et al. 1995; Dimits et al. 1996) and that the

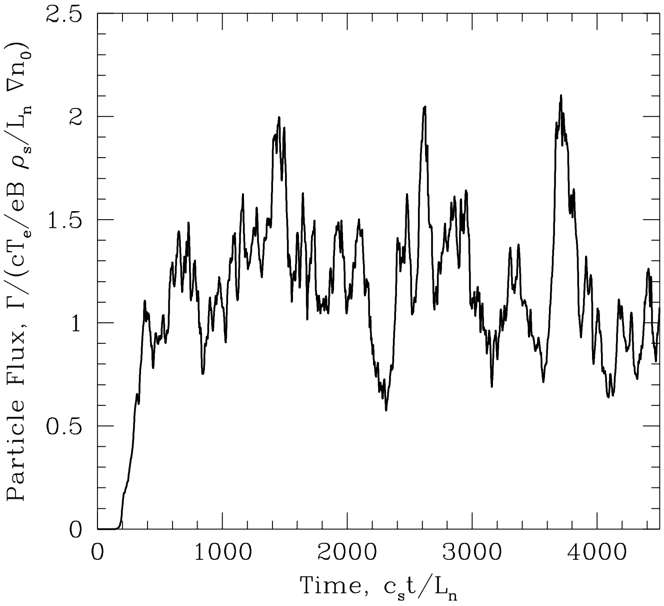


Figure 5.2: Particle flux from simulation of the model equation in a periodic box ($50\rho_s \times 50\rho_s$) in the strong-turbulence regime, $\delta_0 = 0.35$, $\alpha = 0.035$, $\mu = 0.0001$.

saturation amplitude is independent of the size of the simulation domain indicates that a gyro-Bohm scaling regime exists for sufficiently small $\rho_s/L$.) The time history of the flux for a typical set of parameters is shown in Fig. 5.2.

Since observable physical quantities such as the particle flux and mean-square density fluctuations can be expressed as quadratic functions of the potential, one is led to study the evolution and saturation of the squared magnitude of the modes. There is only one quadratic quantity that is conserved by the nonlinear term of the model equation (5.9) corresponding to the fact that the volume-integrated square density, $\int \tilde{n}_i(\mathbf{x})^2\, d\mathbf{x}$, is conserved by divergence-free advection. This conserved quantity is denoted by $\Omega$. A normalized modal contribution to the conserved quantity is defined by

$$\Omega_{\mathbf{k}} = \frac{1}{2}\left[(1+|\mathbf{k}|^2)^2 + {\delta_0}^2 {k_y}^2\right] |\psi_{\mathbf{k}}|^2. \tag{5.15}$$

Fig. 5.3 displays the saturated spectrum for the initial set of parameters, where the standard 2D spectral density is defined by $\Omega(k) = 2\pi k \langle \Omega_{\mathbf{k}} \rangle$, where the average is taken over the band of $\mathbf{k}$'s at radius $k$. (The growth rates for this simulation are displayed in Fig. 5.4.) An attempt to infer an inertial-range power law scaling from

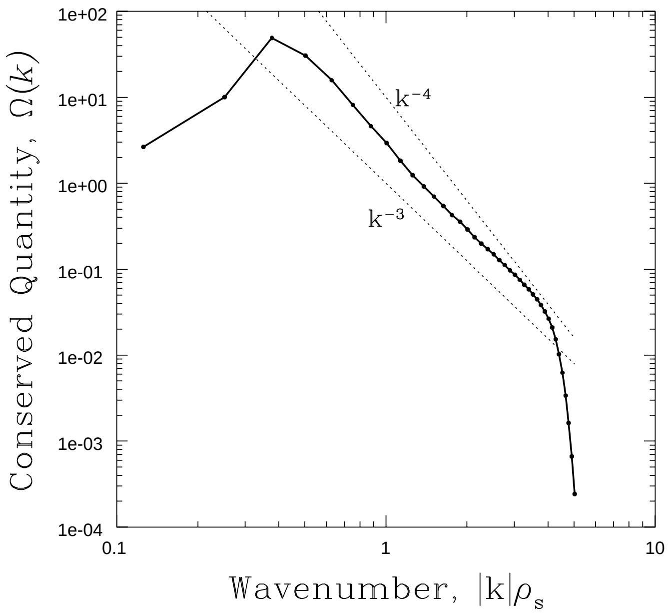


Figure 5.3: Time averaged spectrum of density fluctuations for the simulation of Fig. 5.2.

this spectrum would give $\Omega(k) \sim k^p$ with $-4 < p < -3$, which is very different from the 2D Navier–Stokes high-$k$ inertial range where enstrophy scales as $k^{-1}$ (Kraichnan 1967; Batchelor 1969). In fact, simulations of 2D Navier–Stokes turbulence have typically observed inertial ranges significantly steeper than theoretically predicted. The $k^{-1}$ enstrophy range is an asymptotic limit that can only be observed when the dissipation scales are separated from the forcing scales by at least two orders of magnitude (Borue 1993). The separation of scales required to observe inertial-range scaling is particularly large in 2D turbulence, where the enstrophy transfer is very nonlocal. Such a scenario is highly unlikely for plasma-turbulence problems where significantly damped modes exist at wave numbers very close to the unstable modes driving the turbulence. Therefore, one should not expect to find universal exponents in drift-wave simulations.

The evolution equation for this quadratic invariant is

$$\left(\frac{\partial}{\partial\tau} - 2\gamma_{\mathbf{k}}\right)\Omega_{\mathbf{k}} = T_{\mathbf{k}}, \tag{5.16}$$

where the nonlinear transfer $T_{\mathbf{k}}$ is given by

$$T_{\mathbf{k}} = \left[(1+|\mathbf{k}|^2)^2 + {\delta_0}^2{k_y}^2\right] 2\mathrm{Re}(\psi_{\mathbf{k}}^* N_{\mathbf{k}}). \tag{5.17}$$

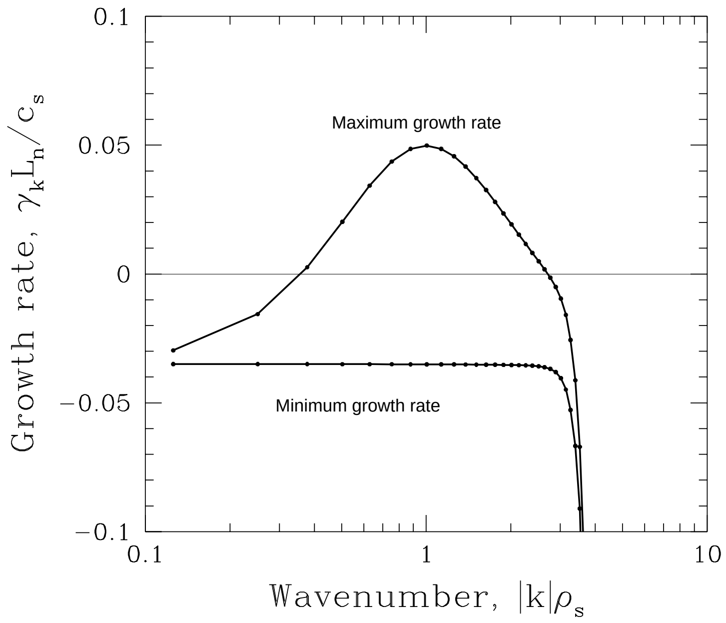


Figure 5.4: Growth rates for the simulation of Fig. 5.2. A $k^{16}$ hyperviscosity damping term has been used to improve the resolution of the inertial range.

In steady state, the nonlinear transfer balances the production and dissipation of fluctuations due to linear growth or damping. (See Fig. 5.5 for a typical example of the linear production.) For 2D equations of this form, with only one quadratic invariant, it has been noted that arguments from statistical mechanics imply transfer to small scales (Diamond and Biglari 1990), in contrast to the dual cascade picture from 2D Navier–Stokes turbulence. With moderate dissipation due to Landau damping at all scales, there is no clearly defined inertial range or cascade. The production of the conserved quantity for a typical run is plotted in Fig. 5.5. Note that the dominant source and the major sink for fluctuation energy both lie near the peak of the spectrum. The major transfer in $\mathbf{k}$ space of fluctuation energy is in fact not a cascade, and takes energy from unstable modes near the $k_x = 0$ axis to Landau-damped modes of nearly the same magnitude near the $k_y = 0$ axis. (Realistic simulations of transport therefore require accurate models of Landau damping.) The dissipation near the cutoff indicates a small cascade of fluctuation energy to high $k$. This picture of energy production in $k$ space is qualitatively similar to that observed in toroidal gyrofluid simulations. [See Fig. 5.9 of Beer (1995).] The small amount of transfer to high $k$ is dynamically insignificant, leading to the conclusion that the level of turbulence is set primarily by eddy turnover at long wavelengths. Simulations of just

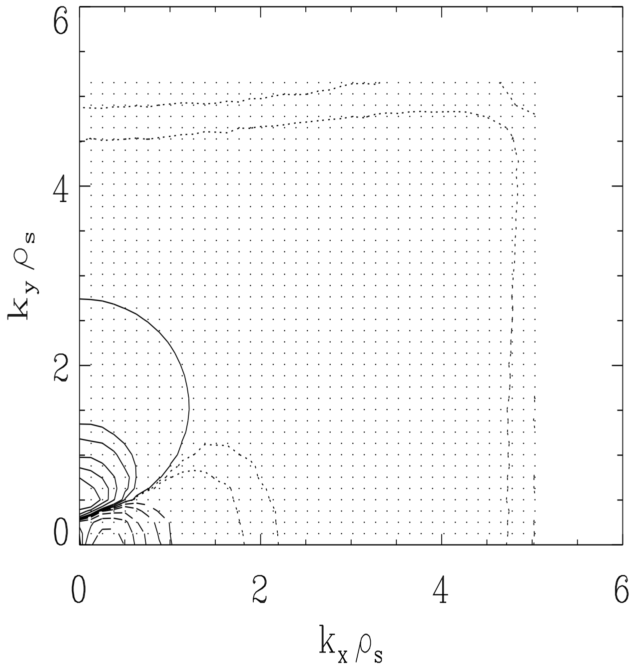


Figure 5.5: Time averaged production and dissipation of density fluctuations for the simulation of Fig. 5.2 (contours of $\langle \gamma_{\mathbf{k}} \Omega_{\mathbf{k}} \rangle$). Each point is a resolved mode. Solid lines are contours of the production region at $0, 1, 2, 5, 10$, and $20$ (dimensionless units). Dashed lines are contours of the dissipation region at $-1, -2, -5, -10$, and $-20$. The dotted lines are contours at $-0.05$ and $-0.1$.

the long wavelengths are therefore theoretically feasible. Simply eliminating modes that lie beyond the bulk of the spectrum can give catastrophic results, however, as the small transfer of fluctuation energy 'piles up' secularly at the cutoff.